A Numerical Study of Important Flow Effects for Quadrotor Performance in Hover

Austin D. Thai,[1] and Sheryl M. Grace[2]
Boston University, Boston, Massachusetts, 02215

Computational fluid dynamics (CFD) simulations of a small quadrotor in hover were conducted using CREATE-AV™ Helios to study the aerodynamics of rotor-fuselage interactions. The effect of fountain flow on hover performance was quantified for a DJI Phantom 3. Ground effect theory is able to describe the reduction in thrust and download as a function of rotor distance for the isolated rotor airframe combination. However, the combination of ground effect and severe flow reingestion for a quadrotor in hover yields a nonlinear relationship between the components of thrust and rotor distance.

I. Nomenclature

R	=	rotor radius
ΔF	=	distance between the rotor and the fuselage arm
ΔC	=	distance between the rotor tip and the cylindrical airframe
S	=	strain rate tensor
Ω	=	rotation rate tensor
Q	=	q-criterion
$\tilde{Q}$	=	q-criterion normalized by rate-of-strain tensor
T_g	=	Thrust in ground effect
T_∞	=	Thrust in free air
v_i	=	Induced velocity at the rotor
δv_i	=	Induced velocity by image
A^*	=	ground effect affected area

II. Introduction

The increasing prevalence of quadrotor usage across various applications such as package delivery, aerial photography, and search and rescue have opened concerns for the design of these small scale aircraft. The quadrotor design procedure has been focused on improving rotor performance by optimizing isolated rotor thrust. However, rotor-rotor and rotor-fuselage interactions play a large role in determining aerodynamic performance. Zawodny et al. studied the effect of single rotor-airframe interactions and demonstrated, for a generic airframe modeled as a cylindrical rod, the thrust level agrees with ground effect theory and decreases as the distance from the airframe increases [1]. However, the interactions of a single rotor with an airframe do not exhibit the fountain flow effect that occurs between multiple rotors. Fountain flow studies have historically focused on large scale helicopters such as the V-22 Osprey Tiltrotor, which has two rotors whose downwash interact with the fuselage. These interactions are well documented and have been predicted as early as Felker and Light, who tested their theory with experiments [2]. An analytical solution of the tiltrotor flowfield by Young and Derby yielded success in deriving the recirculation between the wing and the rotor, and they were able to describe a loss in thrust as the rotors come too closer together [3]. It was at this point that the two main mechanisms of the fountain effect that affect quadrotor performance were identified as download on the fuselage and flow re-ingestion.

Coffen produced flow visualization of the XV-15 tiltrotor using a bubble generator and demonstrated recirculating flow between the rotors and above the wing [4]. Komerath et al. proceeded to study the tiltrotor phenomenon using

[1] Graduate Research Assistant, Department of Mechanical Engineering, AIAA Student Member.
[2] Associate Professor, Department of Mechanical Engineering, and AIAA Member.

spatially correlated velocimetry to capture the velocity field between the rotor blade and the wing experimentally [5]. At the same time, computational fluid dynamics (CFD) gained enough reliability to study tiltrotor aerodynamics, and Potsdam et al. were able to simulateimage flow field results for the first time [6]. Ying et al. were able to continue CFD studies and plotted the streamline distributions of the Osprey at different rotor tilt angles [7]. Recently, Hong was able to predict the coefficient of thrust of the tiltrotor in cross-wind using RotCFD, and flow recirculation from the rotor-fuselage interaction was shown [8]. In general, these past studies were mostly concerned with the V-22 Osprey or XV-15 tilt-rotor, which only has two rotors. Gupta was able to use CFD to simulate a simplified quad tilt rotor vehicle, but these studies nonetheless focus on vehicles that operate at larger length scales than quadrotors [9].

Yoon et al extended the study to small quadrotors and quantified the download on the fuselage [10]. In this same study, Yoon et al changed the rotor-rotor distance to determine the effects on overall performance. Therefore, the relationship between rotor-rotor separation distance and fountain flow is well-documented. However, there have not been studies on fountain flow characterization at different rotor heights. The combination of the effects of download, ground effect, and flow reingestion are studied in this work. Simulations of isolated rotor-airframe and full quadrotor in hover were conducted to characterize fountain flow as a function of rotor height. By varying the rotor height, the fountain flow effect is allowed to further develop because the recirculation region increases in size. However, at a certain point, the wake is able to dissipate, and the performance is expected to approach that of an ideal case in which there is no fuselage. This work will serve the purpose of analyzing aerodynamic interactions between nearby surfaces and multiple rotors and the effect on performance.

III. Methods

A. Computational Model

Simulations were performed using CREATE-AV™ Helios, a parallelizable rotorcraft flow solver that is maintained by the U.S. Army Aviation Development Directorate. Helios is a computational suite that uses a python-based wrapper to modularize its component codes. For example, Helios uses a module called MELODI to handle body motion and define frames of reference. For the flow solution, Helios consists of an overset meshing framework and can couple different near-body solvers with its native off-body solver, SAMCART. SAMCART automatically generates a block-Cartesian volume mesh around geometries of interest and is capable of adaptive mesh refinement. Although Helios is capable of a rotational global reference frame, a stationary global reference frame was used for this study. The domain connectivity and implicit hole cutting is implemented by another module, PUNDIT. For this study, NASA's high-fidelity flow solver FUN3D was used for the near-body solution [11]. FUN3D is an unstructured-grid research code that has been used extensively to study rotorcraft. The combination of Helios with FUN3D will be referred to as "Helios-FUN3D." In both the near-body and off-body, the Reynolds-Averaged Navier-Stokes (RANS) equation is solved with the Spalart-Allmaras Detached-Eddy Simulation (SA-DES) turbulence model [12]. More details on the Helios code can be found in Refs. [13, 14, 15].

B. Problem Definition and Geometry

To study the fountain flow for small quadrotors, two sets of simulations were conducted to study the aerodynamic interactions for both a single rotor-airframe and full quadrotor. In the first set of simulations, the rotor tip distance from a generic cylindrical airframe, ΔC, is varied, as shown in Fig. 1. In the second set, the distance between the rotor hub and the fuselage arm, ΔF, is varied, as shown in Fig 2. The DJI Phantom 3 was chosen for this study because of its commercial success in the unmanned aerial vehicle industry. The DJI Phantom 3 fuselage and rotor geometry was provided by researchers at NASA Ames as shown in Figs. 1-2, with the exception of pins on the fuselage arms. The authors do not expect there to be significant aerodynamic effects from these pins, which are not visible in these images. Note that the camera gimbal, normally included in the DJI Phantom 3 commercial package, is not included. The geometry presented is identical to that tested at NASA Ames Research Center by Russell et al. for the scientific and technical information program [16]. All simulations were conducted with all rotors spinning at 5000 RPM, which is within the operating range of the DJI Phantom 3 and typical for small quadrotors.

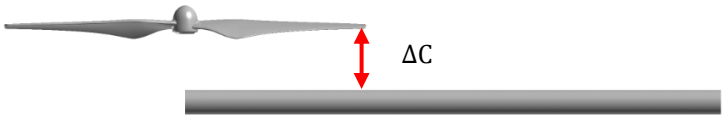

Fig. 1 Rotor distance from cylindrical airframe, ΔC

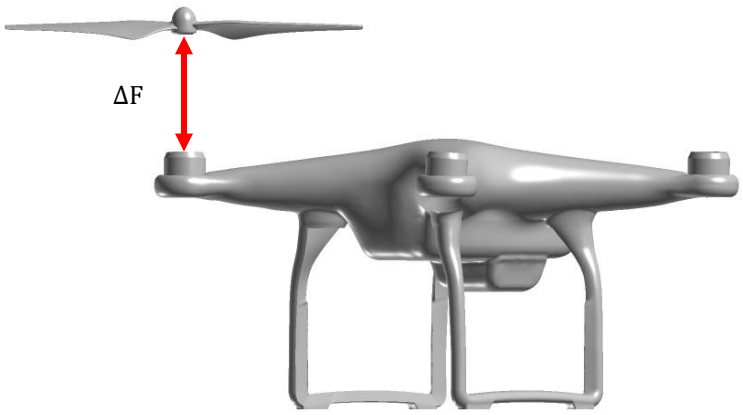

Fig. 2 Rotor distance from fuselage, ΔF

The near-body mesh was generated from the geometries shown using Pointwise's T-Rex algorithm. The near-body volume mesh was trimmed, during runtime, up to 0.4 inches away from the rotor blade and fuselage. The off-body mesh is generated automatically at run time and starts approximately 8 rotor radii away from the fuselage in each direction. The off-body mesh is refined around the geometry of the near-body meshes until the off-body spacing and near-body spacing are similar. Four layers of overlap were set between the near-body and off-body volume meshes. The quadrotor consists of two opposing clockwise and two opposing counterclockwise rotors to provide a natural torque balance. The clockwise and counterclockwise surface meshes have the same properties; either mesh can be created with a mirror image of the other one. The properties of the various meshes can be found Tables 1-3, while close up images of the surface meshes can be seen in Figs. 3-5.

Table 1: Cylinder mesh properties

Radius	0.315 in.
Length	15 in.
Surface spacing	0.05 in.
Volume spacing	0.025 in.
Normal spacing	0.0005 in.
Normal growth rate	1.3
Trim distance	0.4 in.

Table 2: Rotor mesh properties

Radius	4.7241 in.
Surface spacing	0.03 in.
Leading edge spacing	0.0002 in.
Trailing edge spacing	0.0001 in.
Volume spacing	0.03 in.
Normal spacing	0.0001 in.
Normal growth rate	1.1
Trim distance	0.4 in.

Table 3: Fuselage mesh properties

Length (along arm)	15.4 in.
Surface spacing	0.05 in.
Volume spacing	0.05 in.
Normal spacing	0.0005 in.
Normal growth rate	1.3
Trim distance	0.4 in.

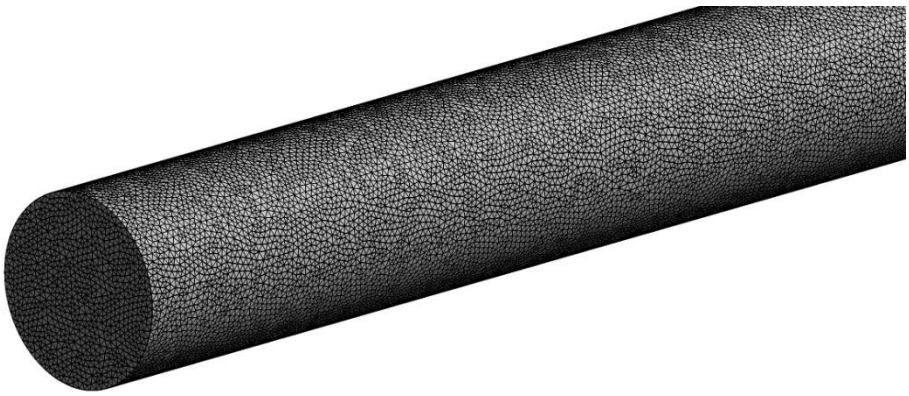

Fig. 3 Cylindrical airframe surface mesh

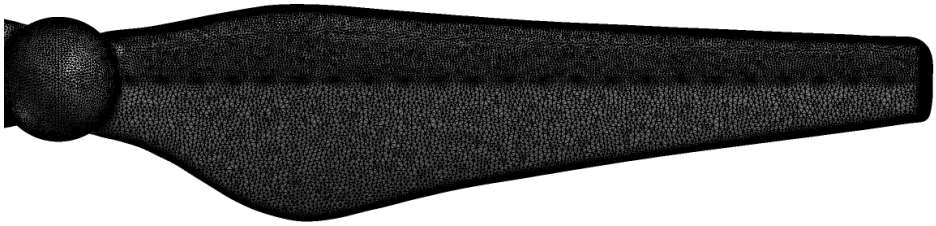

Fig. 4 Rotor surface mesh

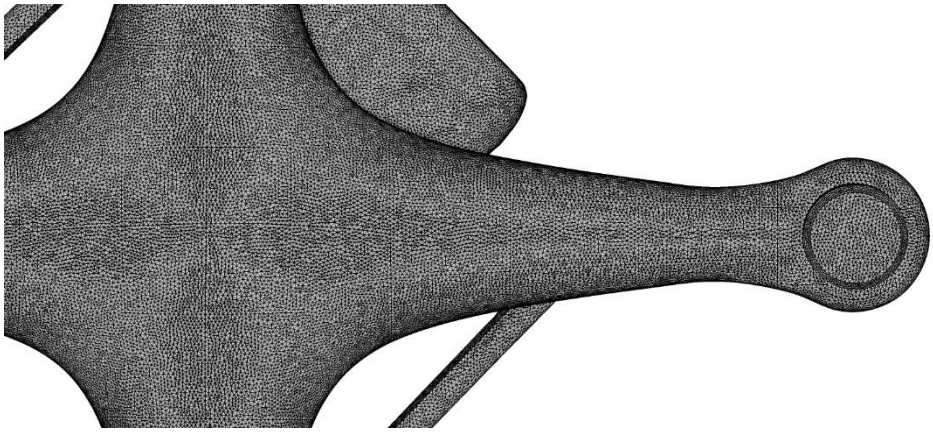

Fig. 5 Fuselage surface mesh

C. Adaptive Mesh Refinement (AMR)

It is possible to create a volume mesh that is incredibly fine at all regions in the flow domain, but the resulting simulation would be very costly and inefficient. Instead, adaptive mesh refinement allows the flow solver to detect interesting flow structures and refine accordingly. The default setting in Helios for adaptive mesh refinement uses a normalized q-criterion, $\tilde{Q}$, as defined by:

$$\tilde{Q} = \frac{1}{2}\left(\frac{||\Omega||^2}{||S||^2} - 1\right), \tag{1}$$

where Ω is the rotation rate tensor and S is the strain rate tensor. The off-body mesh was set to flag regions for refinement where $\tilde{Q} > 1$. This methodology was developed by Kamkar et al. and demonstrates robustness across rotorcraft applications of various spatial and temporal scales [17].

D. Proposed Extension of Ground Effect Theory

By following the theoretical procedures of Cheeseman and Bennett, an estimate of ground effect in hover can be extended by using a simplification of the method of images to one with varying image plane area [18]. At constant power, assuming constant induced velocity by a rotor and its image, the thrust in ground effect can be represented by:

$$T_g = T_\infty \frac{v_i}{v_i - \delta v_i}, \tag{2}$$

where T_∞ is the thrust in free air, v_i is the induced velocity at the rotor, and δv_i is the induced velocity by the image. Typically, the velocity induced by the image is represented by a function of the rotor area:

$$\delta v_i = \frac{A v_i}{16\pi Z^2}. \tag{3}$$

However, the problem definition in this work does not justify using an image plane that occupies the entire rotor area. Instead, an extension of this method is proposed in which the ground effect thrust varies as a function of the ground effect affected area, A*, of the rotor downwash that is impeded by a potential image plane. The newly defined area can be substituted into Eq. 3 and the result into Eq. 2 to derive a relationship between thrust and rotor height:

$$T_g = T_\infty \frac{1}{1 - \frac{A^*}{16\pi Z^2}}. \quad (4)$$

This is essentially the same as predicting the ground effect for a smaller rotor due to a smaller rotor area. This theory will be applied to predict thrust variation for the cylindrical airframe case, in which A* would be represented roughly by the rotor radius multiplied by the cylinder diameter.

IV. Results

A. Single rotor-airframe

Zawodny et al. tested a rotor in hover with a cylindrical airframe both experimentally and computationally with OVERFLOW2 [1]. They were able to demonstrate the ground effect on blade performance and show a decrease in download as a function of height. In this study, these trends were explored using CFD for a similar combination of rotor and cylindrical airframe. The counterclockwise rotor was chosen to agree with the work of Zawodny et al. For the first 10 rotor revolutions, a time step equivalent to 2.5 degree azimuth rotation of the rotor blade was used. For the remainder of the simulation, the time step was changed to 0.25 degree azimuth rotation of the rotor blade. The thrust values were found to converge after 13 rotor revolutions, equivalent to 5760 total time steps. The time stepping methodology was chosen to agree with best practices in rotorcraft CFD. Adaptive mesh refinement was turned on after the first 5 rotor revolutions. Simulations were performed on 640 processors on the Department of Defense high performance computing (DoD-HPC) system Conrad, which has 128 GB Intel Xeon E5-2698v3 compute nodes. As additional validation, isolated rotor thrust results were compared to those found experimentally by Russell et al. and agree within 3% error [16].

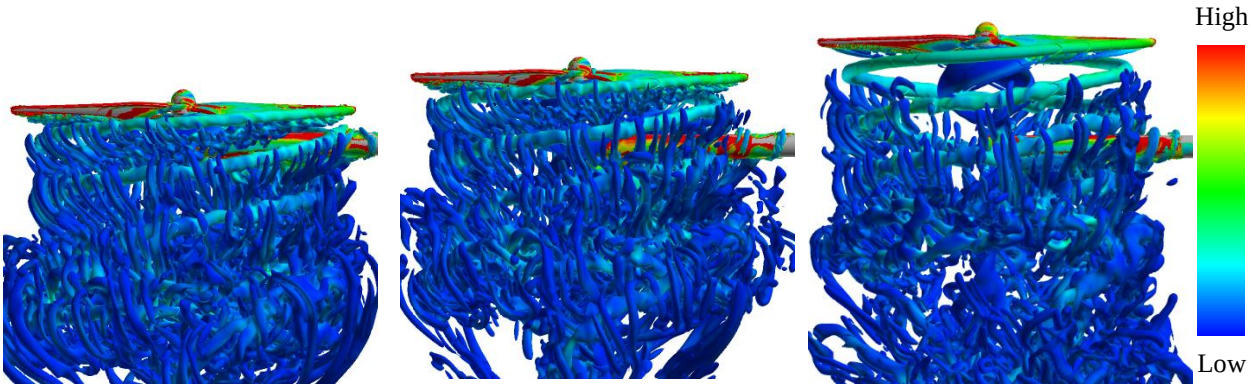

Fig. 6 Instantaneous isosurface of q-criterion colorized by vorticity magnitude for different values of ΔC

In Fig. 6, the isosurface of Q = 0.001 colorized by vorticity magnitude is shown for different rotor-airframe distances. There is a noticeable difference in the amount of vortex structures underneath the case with the greatest ΔC, as expected, due to the decreasing significance of ground effect with height. To quantify these effects, a plot of the calculated thrust from the rotor blade, normalized by isolated rotor thrust, are plotted in Fig. 7 against both theoretical predictions and Zawodny's computations and experiments [1]. The forces integrated over the rotor blades are distinguished from the total forces so that the ground effect on rotor performance can be analyzed separately. The total force is defined as the sum of the blade forces, a positive value that produces thrust, and force on the cylinder, a negative value due to the wake flow impingement. The slight differences between the two computations could be a result of differences in numerical methods. OVERFLOW2 is a structured grid solver and, although Helios uses a structured grid in the off-body, FUN3D was chosen for the near-body and is an unstructured grid solver. In addition, the results may differ because of differences in geometry. Zawodny et al. tested a DJI carbon fiber rotor, while a DJI Phantom 3 rotor is used in this paper [1].

Nonetheless, the same trend can be seen across all studies: rotor performance approaches isolated rotor performance as distance from the airframe increases due to ground effect. Similarly, the download decreases when the rotor is further away because the downwash has more room to develop. The percent change in blade forces from isolated rotor results is minimal, and this can be seen in the figure on the left in Fig. 7. The highest computed difference is around 1.1% and the largest experimental difference around 2.5%. In the case of the isolated rotor-airframe, the

download has the largest impact on thrust. Both computations peak around -8% of the total thrust, which is a significant reduction in performance.

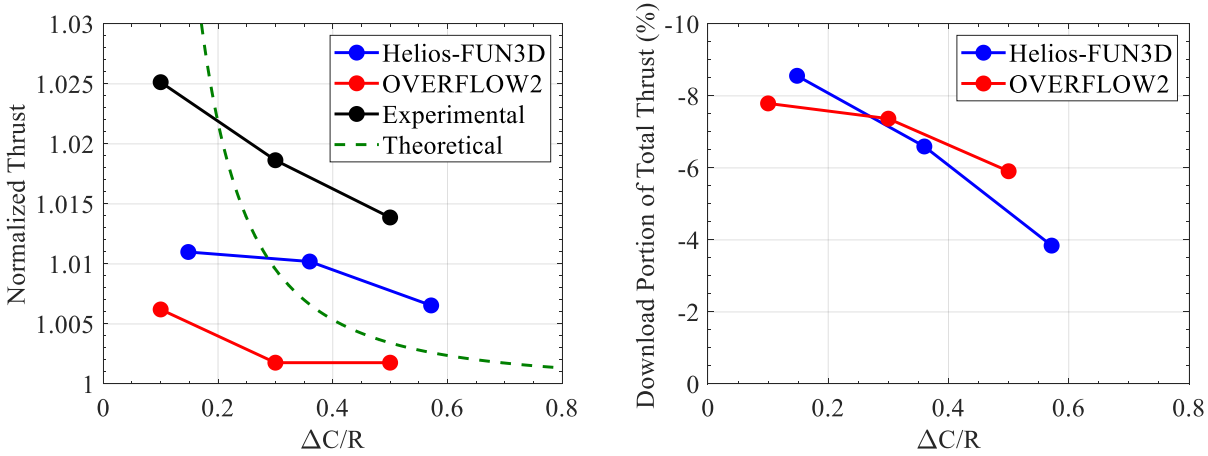

Fig. 7 Integrated thrust over the rotor blade normalized by isolated rotor results (left) and integrated download on the airframe as percentage of total thrust (right) as a function of distance from airframe

B. Quadrotor

In the next set of studies, the rotor height ΔF from the fuselage is varied and the flow field in hover is studied. The time stepping methodology for quadrotor simulations with AMR was adjusted to allow vortices in the wake to impinge upon the fuselage for even the most severe height differences. Quadrotor hover simulations were run with 8 rotor revolutions at 0.25 degree azimuth time steps for a total of 10080 time steps, with AMR turned on after the first rotor revolution. Side views of the cartesian off-body volume mesh with and without AMR can be seen in Figure 8. Without AMR, the wake structures are not well resolved between the rotors and the fuselage, so important flow effects would not be captured. The quadrotor simulations were performed on 960 processors. In Fig. 9a, the total thrust, determined as the sum of the forces on all bodies, was compared to the thrust generated by the blades only. In Fig. 9b, the download on the fuselage was plotted versus the rotor height. Eight cases were run for varying rotor heights and are labeled 1-8 in Fig. 9. Case 1 represents the DJI Phantom 3 configuration most accurately of all cases in this simulation set because the rotor is closest to the fuselage arm. Additionally, to serve as an idealized case, a hover case was run for all four rotors without a fuselage. The thrust results for these two standard cases along with the isolated rotor case can be seen in Table 4. The four independent rotors experienced thrust reduction from rotor-rotor interaction and resulted in a thrust value 3.83 times that of the isolated rotor, while case 1 yielded a thrust of 3.67 times that of the isolated rotor. The interactional aerodynamics demonstrate a large impact on thrust already and this is seen in experiments as well: quadrotor hover results for case 1 were compared to those tested by Russell et al. and agree within 1% error [16].

Table 4: Thrust result comparison for standard cases

	Helios-FUN3D	Experimental
Isolated rotor	0.726 lbf	0.747 lbf
Four rotors (Ideal)	2.7184 lbf	N/A
Quadrotor (Case 1)	2.6679 lbf	2.697 lbf

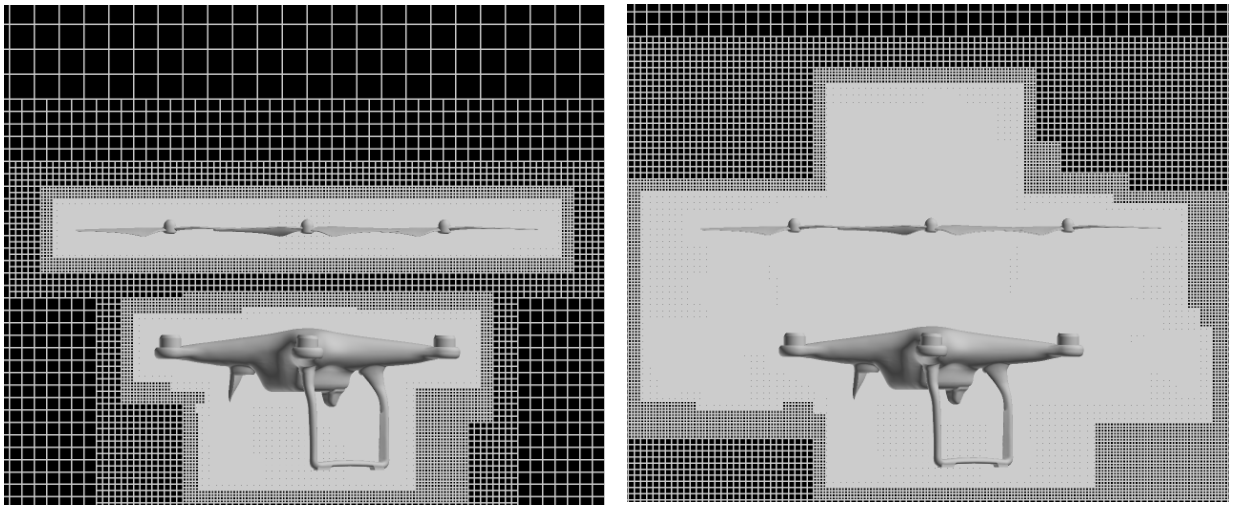

(a) Without AMR (b) With AMR

Fig. 8 Cross section of volume mesh near the quadrotor after 8 rotor revolutions

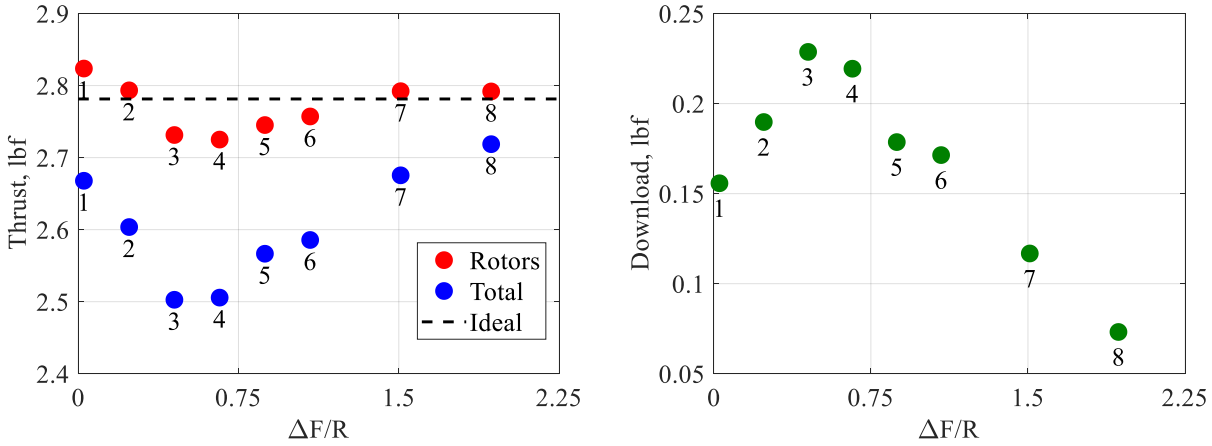

a) Thrust b) Download

Fig. 9 Quadrotor simulation results, points labeled by case number

From Fig. 9a, there is a slight improvement in thrust when the rotors are closest to the fuselage, which occurs as a result of the ground plane. However, ground effect theory alone is not sufficient in describing the flow effects for the quadrotor. In Fig. 10, the isosurface of Q = 0.001 for cases 1 and 3 is shown colorized by vorticity magnitude. There is a noticeably large amount of vorticity at the center of the fuselage above the rotor in case 3 that is not present in case 1. Flow reingestion causes the thrust produced by the rotors to decrease below the ideal case at heights from 0.5R to 1R. The two mechanisms of ground effect and fountain flow are both contributing, and the dip in the thrust on the rotor blades suggest that the reingestion effect dominates for all but the smallest rotor distances. These effects are unnoticeable when the blades are sufficiently far away; the lack of recirculation allows the forces on the blades to stabilize back around the ideal case. These results are specific to the DJI Phantom, but similar trends are expected to be seen in most quadrotors whose fuselage obstruct the rotor downwash.

The total thrust is greatest for case 8, for which the rotor-fuselage distance is greatest, due to a large reduction in download, as shown in Fig. 9b. Therefore, although case 1 enjoys the benefits of ground effect, there is a significant amount of download that prevents the whole system from approaching the total amount of thrust of the ideal case. However, even though it may seem that building quadrotors with high rotors will yield more aerodynamically efficient vehicles, the stability, weight, and drag of the columns required to support these rotors for these systems will be compromised.

Although the download in the isolated rotor-airframe cases decreased as a function of rotor height, the download in the quadrotor case seems to increase at first. This peculiar phenomenon may be a result of fountain flow as well: when the rotors are close to the fuselage, the downwash flows onto and past the fuselage. However, as the rotor height increases, the vortices are able to recirculate and remain in the cushion above the fuselage, causing a high pressure region. Therefore, as the rotor height increases, the download slightly increases. Then, as a critical height is reached, the rotor wake is able to dissipate and circulate around the fuselage. It is interesting to note that, although the effects of download seem to peak at the height of case 3, the effects of flow reingestion seem to cause a trough in the blade forces at case 4. The magnitudes of these variations are very similar, so the total thrust in cases 3 and 4 are almost identical.

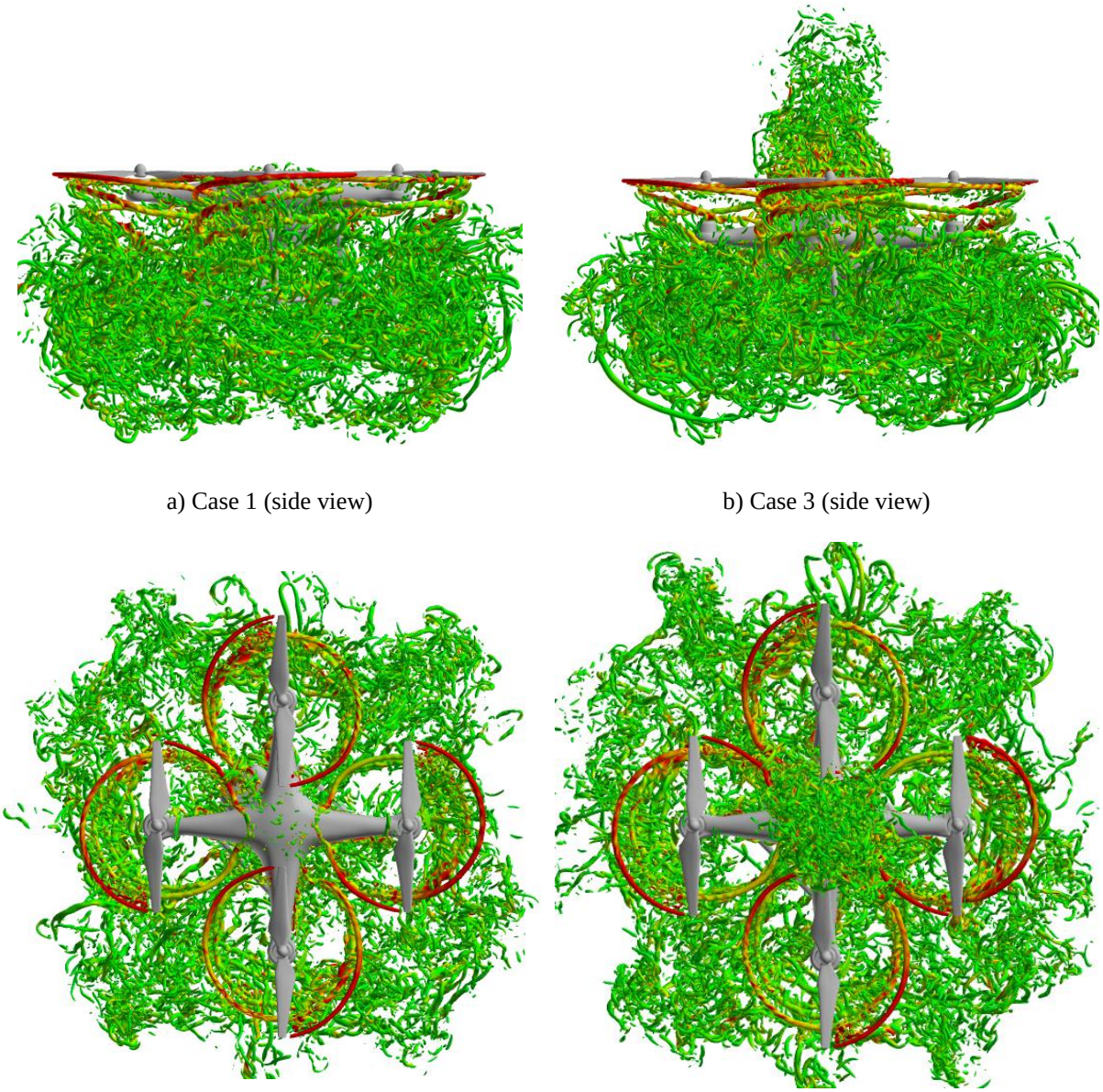

a) Case 1 (side view)

b) Case 3 (side view)

c) Case 1 (top view)

d) Case 3 (top view)

Fig. 10 Isosurface of q-criterion colorized by vorticity magnitude

C. Computational time

The computational time for each set of simulations is plotted in Figs. 11-12. The plots represent the time per time step for each part of the flow solution, such as iBlank checks (orphans and incomplete fringes), the near-body solution, the off-body solution, and domain connectivity. Although the total time is also plotted, other miscellaneous procedures were left out because they were insignificant compared to the components that have been recognized. Although the near-body meshes are the same and the off-body mesh domain is the same for each set, the adaptive mesh refinement will increase the computational time when there are interesting flow structures, thus causing variations in required computational resources. In the isolated rotor-airframe simulations, the time required for each component was relatively unvarying with respect to rotor distance. In the quadrotor simulations, the largest variations were seen in the iBlank checks and the adaptation. The flow field becomes larger as the rotor distance increases, so there is a general upward trend in computational time. The hump in the time required for iBlank checks around 0.25R is caused by a large amount of incomplete fringes.

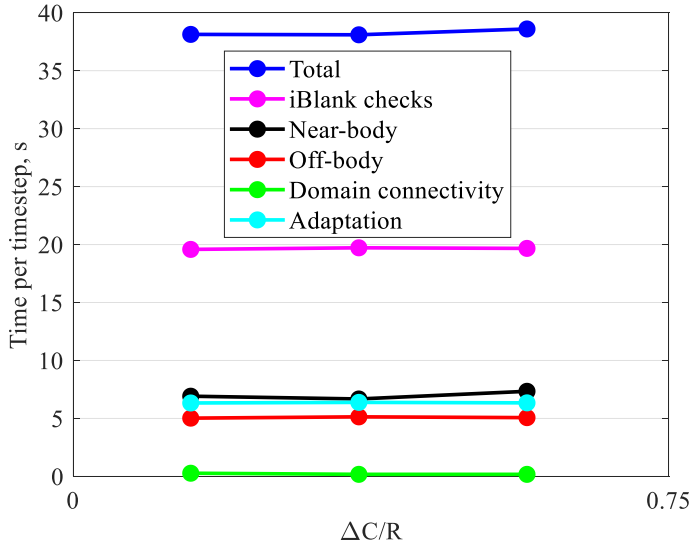

Fig. 11 Time consumed per time step during rotor-airframe simulations for different ΔC

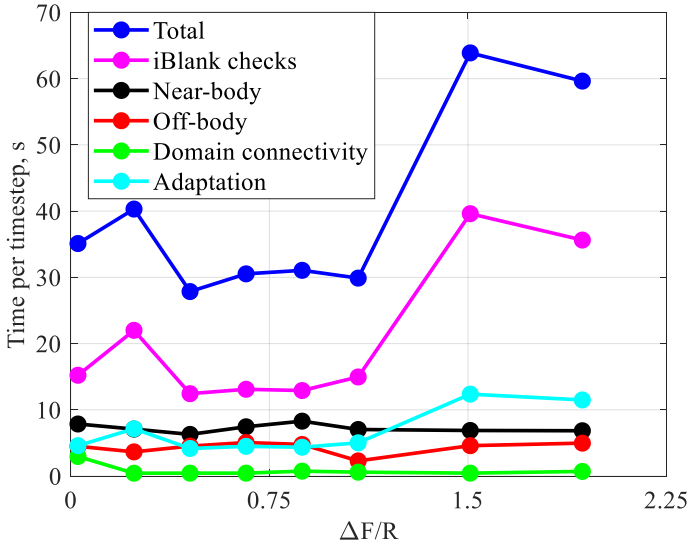

Fig. 12 Time consumed per time step during quadrotor simulations for different ΔF

V. Conclusion

The aerodynamic interactions of a quadrotor were investigated using the computational fluid dynamics code CREATE-AV™ Helios coupled with FUN3D. Simulations of an isolated rotor in hover over a cylindrical airframe were validated against both computational and experimental studies from other works, along with analytical representations of ground effect theory. The download decreased as expected as a function of rotor height, and improved performance was shown when the rotor was in close proximity with the airframe. Then, full quadrotor simulations of the DJI Phantom 3 were performed with two clockwise and two counterclockwise rotors over the fuselage. The standard quadrotor case was shown to provide less thrust than the no-fuselage quadrotors. Due to rotor-rotor interactions, neither of the cases were able to reach 4x isolated rotor thrust.

Next, the distance between the rotors and the fuselage was varied to develop a relationship between rotor height and thrust. Although ground effect theory was sufficient to describe the thrust produced by the isolated rotor and airframe, fountain flow reduced the performance of the quadrotor. For a small regime where the rotors were between 0.5R and 1.0R away from the fuselage, the performance of the rotor blades actually decreased below that of the no-fuselage case. Download and flow reingestion were quantified and, for the set of tests conducted, were shown to peak at different locations. This suggests that the phenomena are connected but distinct, and are a result of the geometry, relative distances, and RPM. It is plausible to imagine a rotor with an exceptional figure of merit that experiences large performance losses in the presence of walls or even other rotors. Therefore, the design process for aerodynamic optimization of quadrotors must include interactional experiments and computations, rather than single rotor studies alone.

This work presents an approach to analyzing important flow effects via a separation of the component forces in the thrust of a quadrotor. However, this study ultimately yields more questions than answers. For example, these computations only studied a quadrotor in hover, and future studies could include gusts and trimmed forward flight to study fountain flow in typical flight conditions. Although aeroacoustics effects were not studied, the significant changes in total performance indicate that the noise generated by a quadrotor will vary as rotor height changes. It is not clear, however, whether performance and sound have a linear relationship as the relative contributions of the rotor, fuselage, and flow field to noise generation must still be studied. This is a key question to answer for design engineers, especially as society anticipates the advent of urban package delivery. Finally, this study demonstrated that changing the rotor height of the DJI Phantom 3 would not provide any immediate performance benefit, but the intricacies of fountain flow suggest that the optimization of the design of a quadrotor should include all aerodynamic interactions.

Acknowledgments

The authors would first like to thank the Boston University Mechanical Engineering department for funding Mr. Thai's studies with a fellowship. The authors thank Carl Russell of NASA Ames Research Center for providing the CAD geometry of the DJI Phantom 3. The authors also thank Rohit Jain, Vinod Lakshminarayan, Steven Tran, Andrew Wissink, Buvana Jayaraman, Beatrice Roget, Mark Potsdam, Jayanarayanan Sitaraman, and Joon Lim for their support in learning the Helios code. Finally, the authors thank Roger Strawn for the opportunity to work with the U.S. Army Aviation Development Directorate and for granting allocations on the Department of Defense high performance computing centers.

References

[1] Zawodny, N. S., and Boyd, D. D., Jr., "Investigation of Rotor-Airframe Interaction Noise Associated with Small-Scale Rotary-Wing Unmanned Aircraft Systems," *73rd American Helicopter Society Forum*, Fort Worth, Texas, 2017.

[2] Felker, F. F., and Light, J. S., "Rotor/Wing Aerodynamic Interactions in Hover," NASA-TM-88255.

[3] Young, L. A., and Derby, M. R., "Rotor/Wing Interactions in Hover," NASA/TM-2002-211392.

[4] Coffen, C. D., "Tilt Rotor Hover Aeroacoustics," NASA-CR-177598.

[5] Komerath, N., Matos, C., and Reddy, U., "Flowfield Issues Related to Tiltrotors," *Tiltrotor/Runway Independent Aircraft Technology and Application Specialists' Meeting of the AHS*, Arlington, Texas, March, 2001.

[6] Potsdam, M., and Strawn, R., "CFD Simulations of Tiltrotor Configurations in Hover," *58th American Helicopter Society Forum*, Montreal, Canada, June, 2002.

[7] Ying, Z., Liang, Ye., and Shuo, Y., "Numerical Study on Flow Fields and Aerodynamics of Tilt Rotor Aircraft in Conversion Mode Based on Embedded Grid and Actuator Model," *Chinese Journal of Aeronautics*, Vol. 28, No. 1, December 2014, pp. 93-102.

[8] Hong, J. W., "Analysis of Fountain Effect for Tiltrotor Configuration Using Computational Fluid Simulation and Experimental Method," M.S. Thesis, Dept. of Aerospace Engineering, Univ. of Illinois at Urbana-Champaign, Urbana, IL, 2017.

[9] Gupta, V., "Quad Tilt Rotor Simulations in Helicopter Mode using Computational Fluid Dynamics," Ph.D. Thesis, Dept. of Aerospace Engineering, Univ. of Maryland, College Park, MD, 2005.

[10] Yoon, S., Lee, H. C., and Pulliam T. H., "Computational Analysis of Multi-Rotor Flows," *54th AIAA Aerospace Sciences Meeting*, San Diego, CA, 2016.

[11] Jain, R., Biedron, R. T., Jones, W. T., and Lee-Rausch, E. M., "Modularization and Validation of FUN3D as a CREATE-AV Helios Near-body Solver" *54th AIAA Aerospace Sciences Meeting*, San Diego, CA, 2016.

[12] Spalart, P., "Detached-Eddy Simulation," *Annual Review of Fluid Mechanics*, Vol. 41, January 2009, pp. 181-202. doi: 10.1146/annurev.fluid.010908.165130.

[13] Sankaran, V., Wissink, A., Datta, A., Sitaraman, J., Jayaraman, B., Potsdam, M., Katz, A.,Kamkar, S., Roget, B., Mavriplis, D., Saberi, H., Chen, W., Johnson, W., and Strawn, R., "Overview of the Helios Version 2.0 Computational Platform for Rotorcraft Simulations," *49th AIAA Aerospace Sciences Meeting*, Orlando, FL, 2011.

[14] Wissink, A., "An Overset Dual-Mesh Solver for Computational Fluid Dynamics," *Seventh International Conference on Computational Fluid Dynamics*, Big Island, Hawaii, 2012.

[15] Wissink, A., Staruk, W., Tran, S., Roget, B., Jayaraman, B., Sitaraman, J., and Lakshminarayan, V., "Overview of New Capabilities in Helios Version 9.0," *57th AIAA Science and Technology Forum*, San Diego, CA, 2019.

[16] Russell, C., Jung, J., Willink, G., and Glasner, B., "Wind Tunnel and Hover Performance Test Results for Multicopter UAS Vehicles," NASA/TM-2018-219758.

[17] Kamkar, S., Wissink, A., Sankaran, V., and Jameson, A., "Feature-driven Cartesian adaptive mesh refinement for vortex-dominated flows," *Journal of Computational Physics*, Orlando, FL, 2010.

[18] Cheeseman, I., and Bennett, W., "The effect of the ground on a helicopter in forward flight," Aeronautical Research Council R. & M. No. 3021.